HHS Public Access

Author manuscript

J Bone Miner Res. Author manuscript; available in PMC 2018 May 01.

Published in final edited form as:

J Bone Miner Res. 2017 May ; 32(5): 892–901. doi:10.1002/jbmr.3038.

Sclerostin antibody administration converts bone lining cells into active osteoblasts

Sang Wan Kim[1,*], **Yanhui Lu**[2,*], **Elizabeth A. Williams**[2], **Forest Lai**[3], **Ji Yeon Lee**[1], **Tetsuya Enishi**[2], **Deepak H. Balani**[2], **Michael S. Ominsky**[4,5], **Hua Zhu Ke**[4,6], **Henry M. Kronenberg**[2,#,^], and **Marc N. Wein**[2,#,^]

[1]Department of Internal Medicine, Seoul National University College of Medicine and Boramae Medical Center, Seoul, Republic of Korea

[2]Endocrine Unit, Massachusetts General Hospital, Harvard Medical School, Boston, MA

[3]Henry M. Goldman School of Dental Medicine, Boston University, Boston, MA

[4]Department of Metabolic Disorders, Amgen Inc., Thousand Oaks, CA

Abstract

Sclerostin antibody (Scl-Ab) increases osteoblast activity, in part through increasing modeling-based bone formation on previously quiescent surfaces. Histomorphometric studies have suggested that this might occur through conversion of bone lining cells into active osteoblasts. However, direct data demonstrating Scl-Ab-induced conversion of lining cells into active osteoblasts is lacking. Here, we used *in vivo* lineage tracing to determine if Scl-Ab promotes the conversion of lining cells into osteoblasts on periosteal and endocortical bone surfaces in mice. Two independent, tamoxifen-inducible lineage tracing strategies were used to label mature osteoblasts and their progeny using the DMP1 and osteocalcin promoters. Following a prolonged 'chase' period, the majority of labeled cells on bone surfaces assumed a thin, quiescent morphology. Then, mice were treated with either vehicle or Scl-Ab (25 mg/kg) twice over the course of the subsequent week. After sacrifice, marked cells were enumerated, their thickness quantified, and proliferation and apoptosis examined. Scl-Ab led to a significant increase in the average thickness of labeled cells on periosteal and endocortical bone surfaces, consistent with osteoblast activation. Scl-Ab did not induce proliferation of labeled cells, and Scl-Ab did not regulate apoptosis of labeled cells. Therefore, direct reactivation of quiescent bone lining cells contributes to the acute increase in osteoblast numbers following Scl-Ab treatment in mice.

Keywords

osteoblasts; molecular pathways–remodeling; Wnt/β-catenin/LRPs; anabolics; preclinical studies

[^]corresponding authors: Endocrine Unit, Massachusetts General Hospital, Thier 1101, 50 Blossom Street, Boston, MA 02114, hkronenberg@partners.org, mnwein@mgh.harvard.edu.

[5]Current address: Radius Health Inc., Waltham, MA

[6]Current address: New Medicines, UCB Pharma, Slough, UK

[*,#]equal contributions

Conflict of interest

Amgen Inc. funded this study. MSO and HZK were employees of Amgen Inc. HZK is currently an employee of UCB.

Introduction

Osteoblasts ultimately undergo one of three fates: they can die by apoptosis, become ensconced within mineralized matrix as osteocytes, or remain quiescent on bone surfaces as bone lining cells (1, 2). Osteoporosis therapies that increase osteoblast activity may do so by multiple potential mechanisms; one rapid pathway to increase bone formation by osteoblasts is via direct conversion of quiescent bone lining cells into active osteoblasts. This pathway has long been posited to be important for how intermittent parathyroid hormone (PTH) treatment rapidly increases osteoblast numbers (3). We recently employed lineage tracing to prove that intermittent PTH administration converts the phenotype of quiescent lining cells to that of active bone-forming osteoblasts (4).

Sclerostin, encoded by the SOST gene, is an osteocyte-derived negative regulator of bone formation (5). Mutations in or near SOST are responsible for the human skeletal dysplasias sclerosteosis and Van Buchem disease (6, 7), and common polymorphisms in SOST have been linked to bone density variation and fracture risk through genome wide association studies (8, 9). Acting as a canonical WNT pathway inhibitor, sclerostin tonically inhibits bone formation by osteoblasts (10). Manipulations, such as mechanical loading (11) and treatment with intermittent PTH (12), that increase bone formation do so in part by reducing SOST expression by osteocytes (13, 14). However, the precise molecular and cellular mechanisms through which sclerostin controls osteoblast differentiation and function remain incompletely understood.

Sclerostin antibody (Scl-Ab) has emerged as a promising therapeutic option for the treatment of osteoporosis. Scl-Ab administration results in activation of bone formation in rodents, cynomolgus monkeys, and humans (15–18). Scl-Ab dramatically increases bone formation on previously-quiescent surfaces, so-called modeling-based bone formation, in rats and cynomolgus monkeys (19). The initiation of modeling-based bone formation by Scl-Ab either occurs through recruitment of new osteoblasts to a quiescent surface or by direct activation of previously-quiescent bone lining cells. Indeed, stereologic histomorphometric analyses have demonstrated concomitant decreases in lining cells and increases in osteoblasts after Scl-Ab treatment in rat trabecular bone (20). However, this methodology does not definitively prove conversion of lining cells into active osteoblasts, nor does it reflect the effects of Scl-Ab in cortical bone. To better understand the possible effects of Scl-Ab on lining cell activation, we conducted a lineage tracing study in mice to label lining cells prior to administration of Scl-Ab and examine their subsequent fate.

Methods

Mice

Temporally-controlled transgene expression was used to trace cells of the osteoblast lineage using *Dmp1*-CreERt2 and Rosa26R mice as previously described (4, 21). *Dmp1*-CreERt2 mice were crossed with Rosa26R mice in which expression of *Escherichia coli* β-galactosidase can be induced by Cre-mediated recombination using a universally expressed promoter (22). These studies were approved by the Institutional Animal Care and Use Committee of Seoul National University. Male and female mice were used for these studies.

Osteocalcin-CreERt2 mice (23) were crossed with B6.Cg-Gt(ROSA)26Sor$^{tm9(CAG-tdTomato)Hze}$I (Ai9) tdTomato reporter mice (24) from the Jackson Laboratory (Bar Harbor, Maine) and osteocalcin-GFP mice (25, 26). These studies were approved by the Massachusetts General Hospital IACUC. Female mice were used for studies with osteocalcin-CreERt2 mice. Animals were housed together, fed standard chow, under 12 hour light/dark cycles. Genotyping primers and protocols are available upon request.

Tamoxifen administration

For experiments with DMP1-CreERt2:Rosa26R mice, 4-hydroxy-tamoxifen was used. For 4-OHTam injections, 2.5 mg of 4-OHTam (Takeda, Osaka, Japan) was dissolved in 100 μl of dimethylformamide (Fisher Scientific, Waltham, MA, USA) and then diluted to 2.5 mg/ml in corn oil (Sigma, St. Louis, MO). *Dmp1*-CreERt2:Rosa26R mice were injected with 0.5 mg 4-OHTam on postnatal week 4, 5, 6, 7 and 8.

For experiments with Osteocalcin-CreERt2:Ai9 mice, mice were injected with 1.0 mg tamoxifen on postnatal week 10. Tamoxifen (Sigma, T5648) was dissolved in 100% ethanol. This solution was mixed with an equal volume of sunflower seed oil (Sigma S5007) and incubated at 60C overnight in a chemical hood until the ethanol completely evaporated. The tamoxifen-oil mixture was then stored at room temperature until use.

Sclerostin antibody administration

Mice were injected subcutaneously with vehicle (phosphate buffered saline) or 25 mg/kg sclerostin antibody (ratized Scl-Ab; Amgen Inc., Thousand Oaks, CA; UCB, Brussels, Belgium) twice over the course of a week. For experiments with DMP1-CreERt2:Rosa26R mice, Scl-Ab was administered 4 weeks after the last tamoxifen treatment (12 weeks of age). For experiments with osteocalcin-CreERt2:Ai9 mice, vehicle or Scl-Ab was administered 5 weeks after the last tamoxifen treatment (15 weeks of age). Mice were randomly allocated into each treatment group.

Histology, X-gal staining and cell thickness measurement

X-gal staining for β-galactosidase activity was performed on sections from DMP1-CreERt2:Rosa26R mice as reported previously (27). Briefly, calvaria and long bones were dissected from the mice, and all soft tissues were removed. Each sample was rinsed twice with PBS, fixed in 10% formalin for 30 min at 4 °C, washed three times with PBS, and then stained overnight at 37 °C in X-gal solution containing 1 mg/ml X-gal (Takeda, Osaka, Japan), 5 mM potassium ferricyanide, 5 mM potassium ferrocyanide, 2 mM $MgCl_2$, 0.01% sodium deoxycholate, and 0.02% Nonidet P-40. Samples were decalcified with buffered EDTA for 2 weeks, and then embedded and processed for paraffin sectioning. Sections were counterstained with eosin. X-gal (+) cells were examined using 3–4 comparable sections and 9–12 fields from each section under 400× from variable numbers of mice per experiment, as indicated in the figure legends. Periosteal X-gal (+) cells from each femur were analyzed using Leica Application Suite camera (DM 2500) and software (LAS V3.8).

Detection of tdTomato and cell thickness measurement

Soft tissue from tibiae was removed and bones were fixed in 4% paraformaldehyde overnight at 4C, then decalcified in 15% EDTA for 21 days. Decalcified samples were cryoprotected in 30% sucrose/PBS solutions and then in 30% sucrose/PBS:OCT (1:1) solution overnight at 4C. Samples were embedded in OCT compound (TissueTek, Sakura) and transferred onto a sheet of dry ice. Embedded samples were cryosectioned at 15 μm using a cryostat (Leica CM1850). Images were captured with a wide-field fluorescence microscope (Nikon Eclipse E800) using triple-band filter setting for DAPI/FITC/TRITC, and merged with Spot Advanced Software. Confocal images were acquired using LSM510 software (Zeiss) with lasers and bandwidth filters for DAPI (excitation 405 nm, BP420–480), GFP (excitation 488 nm, BP505–530), tdTomato (excitation 543, BP565–595), and Alexa633 (excitation 633 nm, LP650). LSM Image Viewer software was used to capture images, Adobe Photoshop was used to align images. Representative images from groups including least 5 independent biological samples are shown in the figures.

For experiments with osteocalcin-CreERt2:Ai9 mice, high power (400x) confocal images of all tomato positive cells on endosteal surfaces on 3 sections per mouse were obtained. Images were coded and imported into ImageJ, and thickness measured in the orientation perpendicular to the bone surface. All measurements were made by an observer blinded to the experimental conditions.

BrdU/EdU labeling and detection

For experiments with DMP1-CreERt2:Rosa26R animals, mice were injected intraperitoneally with BrdU (5-bromo-2-deoxyuridine, Sigma, St. Louis, MO) at 8 h intervals for 24 h and were sacrificed 6 h after the last injection. Tissues were fixed in 4% (vol/vol) paraformaldehyde, processed, and sectioned by standard procedures. BrdU incorporation into DNA was detected using an anti-BrdU antibody staining kit (Zymed Laboratories, San Francisco, CA). The BrdU labeling index was calculated as the ratio of BrdU-positive nuclei relative to the total nuclei on the corresponding periosteal surface of four independent sections of the femur from four mice.

For experiments with osteocalcin-CreERt2:Ai9 animals, mice were injected with 1 mg 5-ethynyl-2′-deoxyuridine (EdU; Invitrogen A10044) in PBS 4 hours prior to sacrifice. Click-iT imaging kit (Invitrogen C10337) with Alexa Fluor 647-azide was used to detect EdU in cryosections.

Caspase-3 and CD45 Immunohistochemistry

Cryosections were stored at −20C until use. Sections were post-fixed in 4% paraformaldehyde for 15 minutes at room temperature. Sections were then stained with an antibody recognizing cleaved caspase 3 (Cell Signaling, 5A1E, #9664) and CD45 (BD Pharmingen, 30-F11, #550539) following the manufacturer’s instructions. An Alexa 647 goat anti-rabbit secondary antibody was used for detection, and sections were stained with DAPI prior to analysis.

Serum biochemistry

Blood was collected by orbital sinus puncture before animals were sacrificed. Serum levels of the N-terminal propeptide of type I procollagen (P1NP) was measured with ELISA kits from Immunodiagnostic Systems (Fountain Hills, AZ).

Electron microscopic analysis and measurement of cell thickness

For experiments with DMP1-CreERt2:Rosa26R mice, after X-gal staining, calvaria were cut transversely at the mid-sagittal suture, fixed in 2.5% glutaraldehyde, 2.0% paraformaldehyde, 0.025% calcium chloride in 0.1 M sodium cacodylate buffer [pH 7.4], and processed for electron microscopy (EM). The LacZ-positive cells were identified by the deposits of X-gal reaction product in the cytoplasm, which appeared as a heterogeneously distributed black amorphous material (28). Samples were examined with a JSM-7401F scanning EM (JEOL, Japan)

Statistics

All data are presented as mean ± standard error of mean (SEM) as indicated in the figure legends, except for serum P1NP measurements which are shown as mean ± standard deviation (SD). The statistical significance of differences between groups was determined by Student's t-test or ANOVA. P values < 0.05 were accepted as significant.

RESULTS

Scl-Ab treatment acutely increases the thickness of periosteal lacZ+ osteoblast descendants

First, we sought to determine if Scl-Ab administration, like intermittent PTH, can activate quiescent periosteal bone lining cells. The *Dmp1*-CreERt2 transgene is active in osteocytes and a subset of osteoblasts on the surfaces of calvariae and long bones (4, 21, 29). In this system, administration of 4-OHTam induces transient nuclear translocation and CreERt2-mediated gene recombination. Because 4-OHTam activity is detected for only 24 h post-injection (28), this inducible system allows us to mark CreERt2-expressing cells and their descendants genetically and at a particular time.

Figure 1 outlines the protocol used for this first series of experiments. When X-gal staining was performed 2 days after the last 4-OHTam injection, many plump osteoblasts on the periosteal surface of the femur were stained (Fig. 2A, upper left). At 4 weeks after the last 4-OHTam injection (12 weeks of age), the cells became flat on the periosteal surface of the femur, and also showed a decline in numbers (Fig. 2A, upper right).

Most X-gal (+) cells on periosteal surfaces assumed a flattened, quiescent morphology 4 weeks after the last 4-OHTam injection. Therefore, we injected Scl-Ab at this time to determine whether Scl-Ab could change the morphology and activity of the flat bone lining cells. After twice weekly Scl-Ab injections (25 mg/kg/d) for 1 week, cuboidal X-gal (+) cells could easily be detected on the periosteal surface of Scl-Ab-treated mice, while in vehicle-treated mice, X-gal (+) cells appeared still flat (Fig. 2A, lower left and lower right).

The number and thickness of the X-gal (+) cells on the periosteal surface of the bones was quantified 2 days (8w) and 4 weeks (12w) after the last 4-OHTam injection, respectively, and after Scl-Ab (13w_Scl-Ab) or vehicle (13w_vehicle) treatment. 4–6 comparable sections from the bones were selected, and the number and the thickness of X-gal (+) cells were measured. The apparent number of X-gal (+) cells on the periosteal surface of the femur was markedly higher in mice treated with Scl-Ab for 1 week than in mice at 4 weeks after the last 4-OHTam injection and in vehicle-treated mice (Fig. 2B). Furthermore, Scl-Ab markedly increased the thickness of osteoblastic descendants in the periosteum of the femur compared to the thickness before Scl-Ab treatment. (Fig. 2C).

Scl-Ab treatment increases the osteoblast activity but not proliferation rate on the periosteal surface of the femur

As expected, one week of Scl-Ab treatment increased serum levels of P1NP compared to vehicle (Fig. 3A). The observed increase in X-gal (+) cells we observed (Fig. 2B) was not necessarily predicted. To explore the mechanism of this increase, we performed BrdU incorporation assays. Scl-Ab did not increase BrdU incorporation into periosteal X-gal (+) cells (Fig. 3B, C). As a positive control for BrdU labeling, robust staining of small intestine from the same mice is shown in Supplemental Figure 1. Collectively, these data support the hypothesis that Scl-Ab re-activates quiescent lining cells on the periosteal surface to become active osteoblasts. We do not fully understand the mechanisms underlying the apparent Scl-Ab-mediated increase in periosteal X-gal (+) cell numbers, possibilities to account for this phenomenon are reviewed in the Discussion.

Scl-Ab converts quiescent lining cells to active osteoblasts: ultrastructural criteria

Ultrastructural features of the cells lining the periosteal surface were the determined by electron microscopy. EM analysis was performed on transverse sections of the calvaria. Consecutive sections were examined by light microscopy and EM. As shown in Fig. 4, EM of X-gal (+) cells on the periosteal surface of the calvaria from *Dmp1*-CreERt2:Rosa26R mice on 4 weeks after the last 4-OHTam injection (12w) showed the typical morphology of inactive lining cells, with scant endoplasmic reticulum. Scl-Ab resulted in an apparent increase in cell size and in the abundance of intracellular organelles, many of which appeared to be rough endoplasmic reticulum (Fig. 4; 13w_Scl-Ab). X-gal deposits were observed in the cytoplasm, and appeared as randomly distributed black amorphous microcrystalline structures. In contrast, X-gal deposits were not observed in osteoblasts on bone surfaces of Rosa26R mice lacking the *Dmp1*-CreERt2 transgene (Supplemental Figure 2). Thus, the EM analysis supports the hypothesis that short-term Scl-Ab treatment activates lining cells to differentiate into cuboidal osteoblasts that may have robust capacities for protein synthesis.

A lineage tracing system to label endocortical osteoblasts

The DMP1-CreERt2;Rosa26R system allows for robust identification and lineage tracing of periosteal osteoblasts (4). However, very few endocortical and cancellous osteoblasts are labeled using this strain. This may reflect limited penetration of the X-gal staining solution. In addition, X-gal staining typically leads to high background, low intensity signals, difficulty delineating cell boundaries, and an inability to use confocal microscopy for

subsequent analysis. To circumvent these problems, we used an osteocalcin-CreERt2 strain (23) in combination with a conceptually-similar Cre-dependent tdTomato reporter strain, termed Ai9 (24). Here, X-gal staining is not required for detection of Cre-dependent tdTomato expression. As previously reported (23), 2 days following tamoxifen administration, tdTomato expression is easily detectable in osteoblasts on cancellous and endocortical surfaces in tibia of such animals (Supplemental Figure 3A). Importantly, in the absence of tamoxifen, tdTomato expression is not present in these mice (Supplemental Figure 3B).

After chase periods of >4 weeks following tamoxifen administration, the vast majority of tdTomato-positive cells present on bone surfaces had disappeared. However, rare tdTomato-positive cells persisted on endocortical surfaces with a thin, quiescent morphology (Supplemental Figure 3C, D). Quantification of the thickness of these cells demonstrated a significant reduction compared to those endocortical tdTomato-positive cells present 2 days after tamoxifen administration. (Supplemental Figure 3E). We were unable to reliably detect persistent tdTomato-positive cells on cancellous bone surfaces in the tibia after prolonged chase (≤4 cells/section) in these mice. Therefore, this osteocalcin-CreERt2:Ai9 lineage tracing system allows for the study of endocortical bone lining cells. Since Scl-Ab increases modeling-based bone formation and reduces quiescent surfaces at endocortical sites in cynomolgus monkeys (19), we used this system to assess effects of Scl-Ab on murine genetically-labeled endocortical bone lining cells.

Short-term Scl-Ab treatment increases the number and thickness of tdTomato+ osteoblast descendants on the endocortical surface of the tibia

Figure 5 shows the experimental strategy used to assess the effects of Scl-Ab treatment on endocortical bone lining cells. A cohort of female mice were treated with tamoxifen once at 10 weeks of age. 6 mice were sacrificed 5 weeks later. The remaining 12 mice were either treated with vehicle or Scl-Ab (25 mg/kg) twice over the course of the subsequent week. All animals were treated with EdU 4 hours prior to sacrifice to label dividing cells.

As expected, one week of Scl-Ab treatment significantly increased serum P1NP levels (Figure 6A). Representative images showing the tdTomato-positive cells on endocortical bone surfaces in the various treatment groups are shown in Figure 6B. In the 5wk and 6wk +VEH groups, tdTomato-positive osteocytes are observed, along with rare, thin cells present on endocortical surfaces. In contrast, in the 6wk+Scl-Ab group, many plump tdTomato-positive cells are present on bone surfaces. The thicknesses of all endocortical tdTomato-positive cells on 2 tibia sections/mouse were measured for all 18 experimental animals. As shown in Figure 6C, the majority of tdTomato-positive cells in the 5wk and 6wk+VEH groups were quite thin (each data point in the figure represents an individual measured cell). In contrast, cells measured after Scl-Ab treatment appeared thicker, with few thin cells remaining. Mouse #9 in the 6wk+VEH group appeared to have many thick cells, and also showed higher serum P1NP levels. Figure 6D shows the average cell thickness for each mouse across the experimental groups. Scl-Ab treatment significantly increased the average cell thickness measured.

Figure 6E shows the relationship between average cell thickness and serum P1NP across the three different groups of experimental mice. Animals with the most robust serum P1NP response also tended to show a more dramatic increase in tdTomato-positive cell thickness. These results are consistent with the hypothesis that lining cell reactivation contributes to Scl-Ab-mediated increases in bone formation in these mice.

Osteocalcin-CreERt2:Ai9 mice were crossed to an osteocalcin-GFP transgenic reporter strain (25). This strategy affords distinction between cells currently expressing osteocalcin (GFP+), and cells that expressed osteocalcin at one time in their lifespan (tdTomato+). Some of the mice used for these experiments were positive for all 3 transgenes (osteocalcin-CreERt2, Ai9, and osteocalcin-GFP). Figure 7A shows representative merged confocal images from these tri-transgenic mice. Many of the endocortical tdTomato-positive lining cells did not actively co-express osteocalcin at this time point, indicating their more mature quiescent state. Scl-Ab treatment tended to increase the percent of co-expression of GFP in tdTomato-positive endocortical cells, although this result did not meet criteria for statistical significance ($p=0.0616$, Figure 7B), likely due to limited numbers of tri-transgenic experimental mice.

Scl-Ab increases lining cell reactivation without affecting proliferation or apoptosis

Similar to results observed in DMP1-CreERt2:Rosa26R mice, Scl-Ab appeared to increase the numbers of visible tdTomato-positive cells on bone surfaces of Osteocalcin-CreERt2:Ai9 mice. Therefore, we investigated whether this increase in cell number was a consequence of the effects of Scl-Ab proliferation and/or apoptosis. EdU was administered to all mice prior to sacrifice to label proliferating cells. While robust EdU incorporation was noted in bone marrow cells, cells positive for both EdU and tdTomato were not observed in any of the Scl-Ab treated mice (Figure 8A). Immunostaining for activated Caspase 3 (aCasp3), a hallmark of cells undergoing apoptosis (30), was performed in order to determine if Scl-Ab treatment regulates apoptosis of tdTomato-labeled lining cells. While aCasp3-positive cells were present in the bone marrow and growth plate, no aCasp3/tdTomato double positive cells were observed in any of the 18 mice studied here (Figure 8B for representative images). Therefore, apoptosis is not a prominent feature of bone lining cells at steady state, so reduced apoptosis is unlikely to solely account for Scl-Ab-mediataed lining cell reactivation.

Tamoxifen-dependent labeling of bone marrow stromal cells in osteocalcin-CreERt2:Ai9 mice

In the course of these studies, we repeatedly noted the presence of tdTomato-positive cells with a particular reticular appearance in the bone marrow far from bone surfaces. Representative images of their morphologic characteristics are shown in Supplemental Figure 4A. These cells are non-proliferating (Supplemental Figure 4B), and do not express the hematopoietic marker CD45 (Supplemental Figure 4C).

A recent report using the same Cre-dependent Ai9 tdTomato reporter with constitutive osteocalcin-Cre and DMP1-Cre transgenes demonstrated tdTomato-positive bone marrow reticular cells as well (31). Zhang and Link reported that many of these tdTomato-positive bone marrow stromal cells expressed high levels of a GFP transgene under the control of the

CXCL12 promoter, a well-described marker of perivascular stromal cells implicated in mesenchymal/ hematopoietic crosstalk (32). Notably, CXCL12-GFP abundant reticular (CAR) cells may represent an osteoblast precursor population (33). Therefore, the possibility remains that Scl-Ab might increase tdTomato-positive endocortical osteoblasts by recruiting labeled stromal cells to become osteoblasts rather than by reactivating previously quiescent bone lining cells. However, overall numbers of tdTomato-positive bone marrow cells with reticular morphology away from bone surfaces was not affected by Scl-Ab treatment (Supplemental Figure 4D), and conversion of marrow stromal cells to osteoblasts would not explain the diminished number of lining cells observed after Scl-Ab treatment. While not definitive, these data argue that the most likely mechanism through which Scl-Ab increases tdTomato-positive osteoblasts is through lining cell reactivation.

DISCUSSION

Here we used lineage tracing to show that Scl-Ab can stimulate bone lining cells to become active osteoblasts *in vivo*. These results extend previous stereological data demonstrating reduced numbers of quiescent lining cells and concomitant increases in osteoblast numbers in response to Scl-Ab (19, 20).

Using two independent models to label mature osteoblasts and their descendants, here we observe that Scl-Ab administration rapidly increases the thickness of labeled cells on periosteal and endosteal cortical surfaces. The most likely mechanism accounting for these findings is that sclerostin neutralization causes quiescent lining cells to reacquire an osteoblastic phenotype. An implication of this finding is that a physiologic role of tonic sclerostin action in bone may be to maintain lining cells on inactive bone surfaces in a quiescent state. Since intermittent PTH also reactivates lining cells and lowers sclerostin levels in bone (12), it is possible that PTH-mediated lining cell reactivation could occur via reducing sclerostin production by osteocytes.

The molecular mechanisms underlying Scl-Ab-mediated lining cell reactivation remain incompletely understood. Recent transcriptional profiling data on bone cells (osteoblasts, lining cells, and osteocytes) following Scl-Ab treatment may provide some clues (34, 35). For example, lining cells (defined as cells on bone surfaces where fluorochrome label was absent) show rapid activation of canonical WNT target genes and ECM components following Scl-Ab treatment. Future studies will be required to understand how activation of WNT signaling rapidly converts lining cells into osteoblasts.

We acknowledge two important limitations in our study. First, the labeling strategies we have employed are designed to label only a small fraction of all osteoblasts and their lining cell descendants. Therefore, it is impossible for us to determine what percentage of all osteoblasts activated by Scl-Ab derive from bone lining cells versus other sources. Second, we use cell thickness as a proxy measure to assess osteoblast activation. Our current study design did not include simultaneous tetracycline labeling to assess proximity of thick labeled cells to active bone surfaces. In previous studies, we have shown that thick, labeled cells on bone surfaces actively express type I collagen mRNA (4). Importantly, work by Kalajzic and colleagues using a similar approach has shown that thick labeled cells are more likely to be

near active, tetracycline-labeled bone surfaces (36). Therefore, we believe that measurement of genetically labeled cell thickness perpendicular to bone surfaces does serve as a reasonable proxy measure for osteoblast activation.

Mechanisms other than lining cell reactivation may account for Scl-Ab-induced increases in osteoblast number, particularly with extended treatment duration. It is likely that Scl-Ab activated lining cells would become embedded as osteocytes in new bone matrix and require additional precursor recruitment to continue bone formation on a given surface. That being said, we have not prospectively followed the fate of Scl-Ab-activated lining cells over time. With chronic administration, the Scl-Ab mediated increases in bone formation are not sustained, which have been associated with changes in osteocyte gene expression and decreases in osteoprogenitor numbers (35). Reduced apoptosis of existing osteoblasts and stimulation of early pools of osteoblast precursors may participate as well. One interesting hypothesis that emerges from this work is that waning Scl-Ab efficacy over time is due to a dwindling reserve pool of quiescent lining cells that can be activated after repeated Scl-Ab administration. Definitive studies of the effects of Scl-Ab on osteoprogenitor populations will require use of advanced technologies such as flow cytometry and lineage tracing designed to identify, profile, and track such cells over time during the response to Scl-Ab administration.

Using both transgenic lineage tracing models, we observed an apparent increase in the number of labeled cells on bone surfaces following Scl-Ab treatment. This was not accompanied by an obvious increase in cell proliferation (measured by BrdU and EdU incorporation) or a decrease in apoptosis. Changes in these parameters may occur below the detection limits of the methods used. An alternative possibility may be that our detection method for labeled cells on two-dimensional sections is biased towards detection of large cells. Since Scl-Ab clearly increases the size of labeled cells, the increase in cell numbers observed may reflect a technical limitation of our approach rather than a true increase in cell number. Future studies using three-dimensional detection methods (36, 37) will be required to resolve this important issue.

The precise identity of the reticular-appearing bone marrow cells labeled in osteocalcin-CreERt2:Ai9 mice remains elusive. These cells do not express high levels of osteocalcin, as evident by lack of GFP expression in osteocalcin-GFP:osteocalcin-CreERt2:Ai9 tri-transgenic mice 2 days after tamoxifen administration (not shown). This finding does not exclude low osteocalcin expression, or ectopic expression of the osteocalcin-CreERt2 transgene. These cells are not actively dividing (Supplemental Figure 4A), and numbers of these cells are not affected by Scl-Ab treatment (Supplemental Figure 4D). Therefore, it is unlikely that these cells provide a major contribution to the pool of tdTomato-positive osteoblasts observed after Scl-Ab treatment. Furthermore, since Scl-Ab also increases the thickness of labeled periosteal cells, we believe that it is extremely unlikely that these bone marrow reticular cells could migrate across cortical bone to contribute to this population of new osteoblasts.

A distinct, and equally unlikely, possibility to explain these results could be that Scl-Ab treatment could cause labeled osteocytes to de-differentiate into active osteoblasts. Indeed,

this phenomenon has been described to occur in *ex vivo* bone chip explant cultures (39). Overall numbers of X-gal and tdTomato-positive osteocytes are not decreased following brief Scl-Ab treatment (not shown), and osteocyte de-differentiation into osteoblasts has not been reported to occur under physiologic *in vivo* settings.

These findings highlight an inherent limitation associated with *in vivo* lineage tracing studies. If the promoter upstream of a given CreERt2 (or Cre) transgene is initially active in a heterogeneous population of cells, it is difficult to unambiguously identify the source of a labeled cell at the end of a 'chase' period. Just as osteocalcin-driven CreERt2 (our findings) and osteocalcin-Cre (31) label non-osteoblasts, the commonly-used osterix-Cre transgene has been reported to target multiple cell types outside the osteoblast lineage postnatally (39). Nonetheless, our data here using *in vivo* lineage tracing in mice are completely consistent with previous results in rats and cynomolgus monkeys suggesting that Scl-Ab increases osteoblast number in part via converting quiescent lining cells into osteoblasts.

The therapeutic efficacy of both intermittent PTH and Scl-Ab wanes with time, albeit with differing kinetics (18, 41). An appealing hypothesis to account for some of this pattern could be that both treatments quickly consume the pool of quiescent lining cells poised to become osteoblasts. A detailed understanding of how lining cells develop and are subsequently activated will be required to design new agents to enable persistent increases in osteoblastic activity.

Supplementary Material

Refer to Web version on PubMed Central for supplementary material.

Acknowledgments

This study was funded by Amgen Inc. This work is also supported by grants from the NIH: K08AR067285 (MNW), P01DK011794 (HMK), and P30AR066261 (HMK) and Promising-Pioneering Researcher Program through SNU in 2015 and Boramae Medical Center, 01-2014-12 (SWK). All authors designed experiments, interpreted experiments, and edited the manuscript. SWK, YL, EAW, FL, TE, JYL, and MNW performed experiments. DB provided technical advice at the early stage of this project. MNW and HMK wrote the manuscript. MNW and SWK accept responsibility for the integrity of the data analysis.

References

1. Miller SC, de Saint-Georges L, Bowman BM, Jee WS. Bone lining cells: structure and function. Scanning microscopy. 1989 Sep; 3(3):953–60. discussion 60–1. [PubMed: 2694361]
2. Miller SC, Jee WS. The bone lining cell: a distinct phenotype? Calcified tissue international. 1987 Jul; 41(1):1–5.
3. Dobnig H, Turner RT. Evidence that intermittent treatment with parathyroid hormone increases bone formation in adult rats by activation of bone lining cells. Endocrinology. 1995 Aug; 136(8):3632–8. [PubMed: 7628403]
4. Kim SW, Pajevic PD, Selig M, Barry KJ, Yang JY, Shin CS, et al. Intermittent parathyroid hormone administration converts quiescent lining cells to active osteoblasts. Journal of bone and mineral research : the official journal of the American Society for Bone and Mineral Research. 2012 Oct; 27(10):2075–84.
5. Baron R, Kneissel M. WNT signaling in bone homeostasis and disease: from human mutations to treatments. Nature medicine. 2013 Feb; 19(2):179–92.

6. Brunkow ME, Gardner JC, Van Ness J, Paeper BW, Kovacevich BR, Proll S, et al. Bone dysplasia sclerosteosis results from loss of the SOST gene product, a novel cystine knot-containing protein. American journal of human genetics. 2001 Mar; 68(3):577–89. [PubMed: 11179006]
7. Balemans W, Patel N, Ebeling M, Van Hul E, Wuyts W, Lacza C, et al. Identification of a 52 kb deletion downstream of the SOST gene in patients with van Buchem disease. Journal of medical genetics. 2002 Feb; 39(2):91–7. [PubMed: 11836356]
8. Estrada K, Styrkarsdottir U, Evangelou E, Hsu YH, Duncan EL, Ntzani EE, et al. Genome-wide meta-analysis identifies 56 bone mineral density loci and reveals 14 loci associated with risk of fracture. Nature genetics. 2012 May; 44(5):491–501. [PubMed: 22504420]
9. Rivadeneira F, Styrkarsdottir U, Estrada K, Halldorsson BV, Hsu YH, Richards JB, et al. Twenty bone-mineral-density loci identified by large-scale meta-analysis of genome-wide association studies. Nature genetics. 2009 Nov; 41(11):1199–206. [PubMed: 19801982]
10. Li X, Zhang Y, Kang H, Liu W, Liu P, Zhang J, et al. Sclerostin binds to LRP5/6 and antagonizes canonical Wnt signaling. The Journal of biological chemistry. 2005 May 20; 280(20):19883–7. [PubMed: 15778503]
11. Robling AG, Niziolek PJ, Baldridge LA, Condon KW, Allen MR, Alam I, et al. Mechanical stimulation of bone in vivo reduces osteocyte expression of Sost/sclerostin. The Journal of biological chemistry. 2008 Feb 29; 283(9):5866–75. [PubMed: 18089564]
12. Keller H, Kneissel M. SOST is a target gene for PTH in bone. Bone. 2005 Aug; 37(2):148–58. [PubMed: 15946907]
13. Tu X, Rhee Y, Condon KW, Bivi N, Allen MR, Dwyer D, et al. Sost downregulation and local Wnt signaling are required for the osteogenic response to mechanical loading. Bone. 2012 Jan; 50(1): 209–17. [PubMed: 22075208]
14. Kramer I, Loots GG, Studer A, Keller H, Kneissel M. Parathyroid hormone (PTH)-induced bone gain is blunted in SOST overexpressing and deficient mice. Journal of bone and mineral research : the official journal of the American Society for Bone and Mineral Research. 2010 Feb; 25(2):178–89.
15. Li X, Ominsky MS, Warmington KS, Morony S, Gong J, Cao J, et al. Sclerostin antibody treatment increases bone formation, bone mass, and bone strength in a rat model of postmenopausal osteoporosis. Journal of bone and mineral research : the official journal of the American Society for Bone and Mineral Research. 2009 Apr; 24(4):578–88.
16. Ominsky MS, Vlasseros F, Jolette J, Smith SY, Stouch B, Doellgast G, et al. Two doses of sclerostin antibody in cynomolgus monkeys increases bone formation, bone mineral density, and bone strength. Journal of bone and mineral research : the official journal of the American Society for Bone and Mineral Research. 2010 May; 25(5):948–59.
17. Padhi D, Jang G, Stouch B, Fang L, Posvar E. Single-dose, placebo-controlled, randomized study of AMG 785, a sclerostin monoclonal antibody. Journal of bone and mineral research : the official journal of the American Society for Bone and Mineral Research. 2011 Jan; 26(1):19–26.
18. McClung MR, Grauer A, Boonen S, Bolognese MA, Brown JP, Diez-Perez A, et al. Romosozumab in postmenopausal women with low bone mineral density. The New England journal of medicine. 2014 Jan 30; 370(5):412–20. [PubMed: 24382002]
19. Ominsky MS, Niu QT, Li C, Li X, Ke HZ. Tissue-level mechanisms responsible for the increase in bone formation and bone volume by sclerostin antibody. Journal of bone and mineral research : the official journal of the American Society for Bone and Mineral Research. 2014 Jun; 29(6):1424–30.
20. Ominsky MS, Brown DL, Van G, Cordover D, Pacheco E, Frazier E, et al. Differential temporal effects of sclerostin antibody and parathyroid hormone on cancellous and cortical bone and quantitative differences in effects on the osteoblast lineage in young intact rats. Bone. 2015 Dec. 81:380–91. [PubMed: 26261096]
21. Jang MG, Lee JY, Yang JY, Park H, Kim JH, Kim JE, et al. Intermittent PTH treatment can delay the transformation of mature osteoblasts into lining cells on the periosteal surfaces. Journal of bone and mineral metabolism. 2015 Aug 25.
22. Soriano P. Generalized lacZ expression with the ROSA26 Cre reporter strain. Nat Genet. 1999 Jan; 21(1):70–1. Epub 1999/01/23. eng. [PubMed: 9916792]

23. Park D, Spencer JA, Koh BI, Kobayashi T, Fujisaki J, Clemens TL, et al. Endogenous bone marrow MSCs are dynamic, fate-restricted participants in bone maintenance and regeneration. Cell stem cell. 2012 Mar 2; 10(3):259–72. [PubMed: 22385654]
24. Madisen L, Zwingman TA, Sunkin SM, Oh SW, Zariwala HA, Gu H, et al. A robust and high-throughput Cre reporting and characterization system for the whole mouse brain. Nature neuroscience. 2010 Jan; 13(1):133–40. [PubMed: 20023653]
25. Kalajzic Z, Liu P, Kalajzic I, Du Z, Braut A, Mina M, et al. Directing the expression of a green fluorescent protein transgene in differentiated osteoblasts: comparison between rat type I collagen and rat osteocalcin promoters. Bone. 2002 Dec; 31(6):654–60. [PubMed: 12531558]
26. Ono N, Ono W, Nagasawa T, Kronenberg HM. A subset of chondrogenic cells provides early mesenchymal progenitors in growing bones. Nature cell biology. 2014 Dec; 16(12):1157–67. [PubMed: 25419849]
27. Chung UI, Lanske B, Lee K, Li E, Kronenberg H. The parathyroid hormone/parathyroid hormone-related peptide receptor coordinates endochondral bone development by directly controlling chondrocyte differentiation. Proc Natl Acad Sci U S A. 1998 Oct 27; 95(22):13030–5. Epub 1998/10/28. eng. [PubMed: 9789035]
28. Maes C, Kobayashi T, Selig MK, Torrekens S, Roth SI, Mackem S, et al. Osteoblast precursors, but not mature osteoblasts, move into developing and fractured bones along with invading blood vessels. Dev Cell. 2010 Aug 17; 19(2):329–44. Epub 2010/08/17. eng. [PubMed: 20708594]
29. Powell WF Jr, Barry KJ, Tulum I, Kobayashi T, Harris SE, Bringhurst FR, et al. Targeted ablation of the PTH/PTHrP receptor in osteocytes impairs bone structure and homeostatic calcemic responses. J Endocrinol. 2011 Apr; 209(1):21–32. Epub 2011/01/12. eng. [PubMed: 21220409]
30. Nicholson DW, Ali A, Thornberry NA, Vaillancourt JP, Ding CK, Gallant M, et al. Identification and inhibition of the ICE/CED-3 protease necessary for mammalian apoptosis. Nature. 1995 Jul 6; 376(6535):37–43. [PubMed: 7596430]
31. Zhang J, Link DC. Targeting of Mesenchymal Stromal Cells by Cre-Recombinase Transgenes Commonly Used to Target Osteoblast Lineage Cells. Journal of bone and mineral research : the official journal of the American Society for Bone and Mineral Research. 2016 May 30.
32. Calvi LM, Link DC. The hematopoietic stem cell niche in homeostasis and disease. Blood. 2015 Nov 26; 126(22):2443–51. [PubMed: 26468230]
33. Zhou BO, Yue R, Murphy MM, Peyer JG, Morrison SJ. Leptin-receptor-expressing mesenchymal stromal cells represent the main source of bone formed by adult bone marrow. Cell stem cell. 2014 Aug 7; 15(2):154–68. [PubMed: 24953181]
34. Nioi P, Taylor S, Hu R, Pacheco E, He YD, Hamadeh H, et al. Transcriptional Profiling of Laser Capture Microdissected Subpopulations of the Osteoblast Lineage Provides Insight Into the Early Response to Sclerostin Antibody in Rats. Journal of bone and mineral research : the official journal of the American Society for Bone and Mineral Research. 2015 Aug; 30(8):1457–67.
35. Taylor S, Ominsky MS, Hu R, Pacheco E, He YD, Brown DL, et al. Time-dependent cellular and transcriptional changes in the osteoblast lineage associated with sclerostin antibody treatment in ovariectomized rats. Bone. 2016 Mar.84:148–59. [PubMed: 26721737]
36. Treweek JB, Chan KY, Flytzanis NC, Yang B, Deverman BE, Greenbaum A, et al. Whole-body tissue stabilization and selective extractions via tissue-hydrogel hybrids for high-resolution intact circuit mapping and phenotyping. Nature protocols. 2015 Nov; 10(11):1860–96. [PubMed: 26492141]
37. Yang B, Treweek JB, Kulkarni RP, Deverman BE, Chen CK, Lubeck E, et al. Single-cell phenotyping within transparent intact tissue through whole-body clearing. Cell. 2014 Aug 14; 158(4):945–58. [PubMed: 25088144]
38. Torreggiani E, Matthews BG, Pejda S, Matic I, Horowitz MC, Grcevic D, et al. Preosteocytes/osteocytes have the potential to dedifferentiate becoming a source of osteoblasts. PloS one. 2013; 8(9):e75204. [PubMed: 24040401]
39. Chen J, Shi Y, Regan J, Karuppaiah K, Ornitz DM, Long F. Osx-Cre targets multiple cell types besides osteoblast lineage in postnatal mice. PloS one. 2014; 9(1):e85161. [PubMed: 24454809]

40. Tsai JN, Uihlein AV, Lee H, Kumbhani R, Siwila-Sackman E, McKay EA, et al. Teriparatide and denosumab, alone or combined, in women with postmenopausal osteoporosis: the DATA study randomised trial. Lancet. 2013 Jul 6; 382(9886):50–6. [PubMed: 23683600]

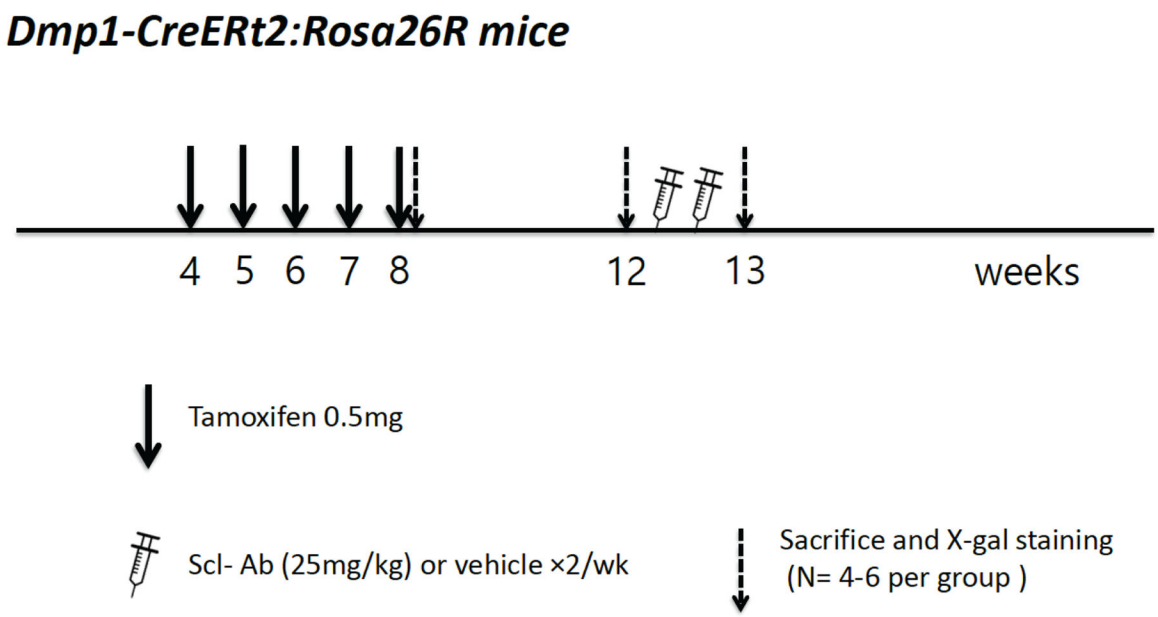

Figure 1. Experimental protocol: DMP1-lineage periosteal lining cells

Dmp1-CreERt2:Rosa26R mice were injected with 0.5 mg 4-OHTam on postnatal week 4, 5, 6, 7 and 8. Animals were sacrificed on postnatal week 8 or 12 (2 days or 4 weeks after the last 4-OHTam treatment), as well as on week 13 to evaluate the actions of Scl-Ab administration.

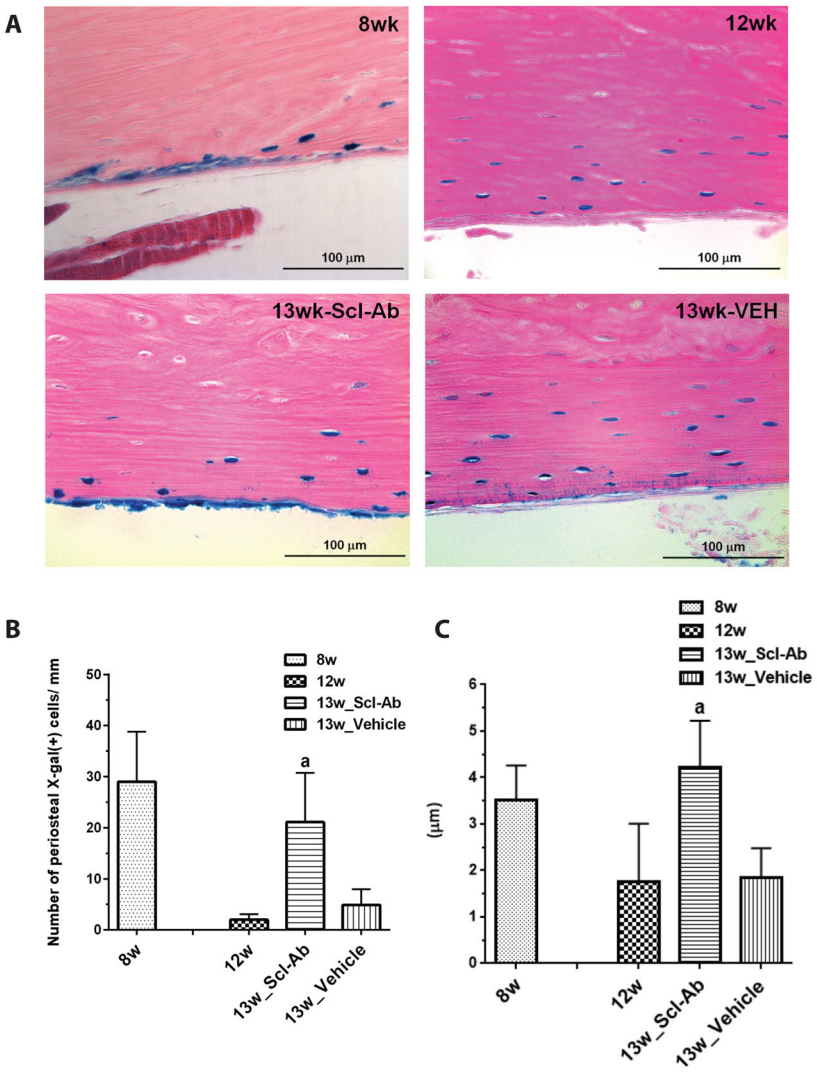

Figure 2. Effects of Scl-Ab on LacZ+ osteoblast descendants on the periosteal surface of the femur

(A) X-gal staining was performed at 2 days (8w) or 4 weeks (12w) after the last 4-OHTam injection, or animals were injected with Scl-Ab (25 mg/kg/d) (13w_Scl-Ab) or vehicle (13w_vehicle) twice a week. Data are representative of experiments performed on sections from six mice for each group. Quantitative analysis of the number **(B)** and thickness **(C)** of X-gal (+) cells before and after Scl-Ab or vehicle treatment. Data are expressed as mean ± SEM, a: $p < 0.05$ versus 12w or 13w_vehicle. The mean cell number and thickness were determined in 3–4 comparable sections per mouse, viewing 9–12 fields/section under 400× from six mice per each group.

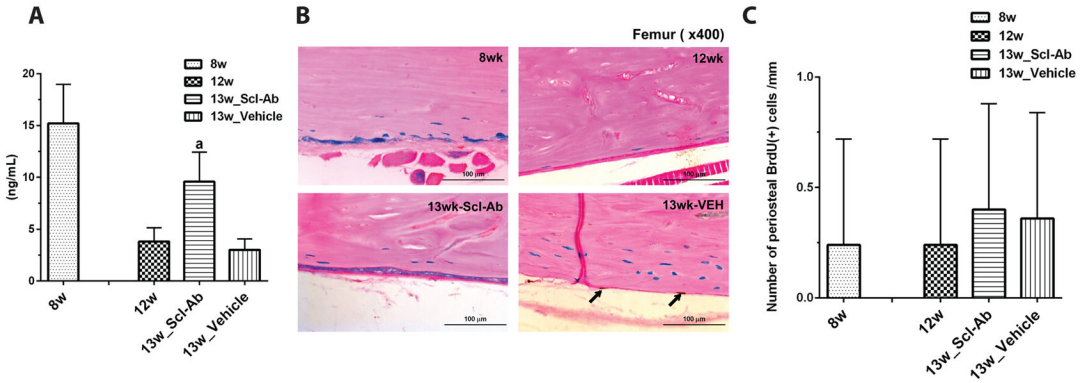

Figure 3. The effect of Scl-Ab on BrdU incorporation and osteogenic activity

(A) The levels of serum P1NP for *Dmp1*-CreERt2:Rosa26R mice receiving Scl-Ab or vehicle treatment for 1 week. Data are expressed as mean ± SD, n = 4; a: $p < 0.05$ versus 12w or 13w_vehicle.

(B) BrdU incorporation analysis for *Dmp1*-CreERt2:Rosa26R mice receiving Scl-Ab or vehicle treatment for 1 week. BrdU staining of paraffin sections of the femur was performed (middle panel). No X-gal (+) cell shows BrdU staining. **(C)** The mean number of BrdU-positive cells (arrows in panel B) was determined in 3–4 comparable sections, viewing 9–12 fields/section under 400× from four mice per each group (right panel). Data are expressed as mean ± SEM. Data are representative of experiments performed on sections from three mice for each group.

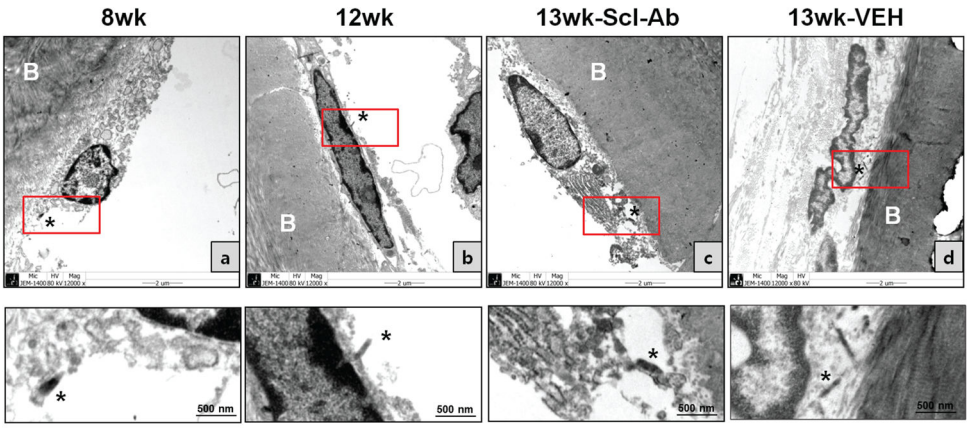

Figure 4. Electron microscopy analysis of the effect of Scl-Ab on LacZ (+) osteoblastic descendants on the periosteal surface of the calvaria

X-gal stained calvarial bones were sectioned at 1μm thickness to visualize tissue morphology and to align X-gal staining with EM imaging. EM analysis was performed at 2 days (a: 8w) and 4 weeks (b: 12w) after the last 4-OHTam or after Scl-Ab (c) or vehicle (d) treatments twice a week. Each lower panel shows a magnified image of the red box in the upper panel. X-gal deposits in the cytoplasm of LacZ+ cells were visible by EM as black amorphous material (asterisk). Data are representative of experiments performed on sections from four mice for each group.

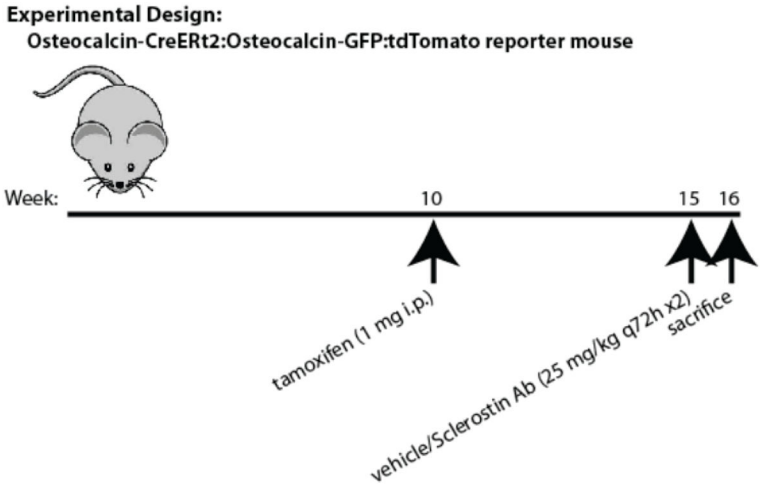

Figure 5. Experimental protocol: osteocalcin-lineage endocortical lining cells

Osteocalcin-CreERt2:Ai9:osteocalcin-GFP mice were injected with 1 mg tamoxifen on postnatal week 10. Animals were sacrificed on postnatal week 15 (5wk) or 16 following a week of vehicle or Scl-Ab (25 mg/kg) administration.

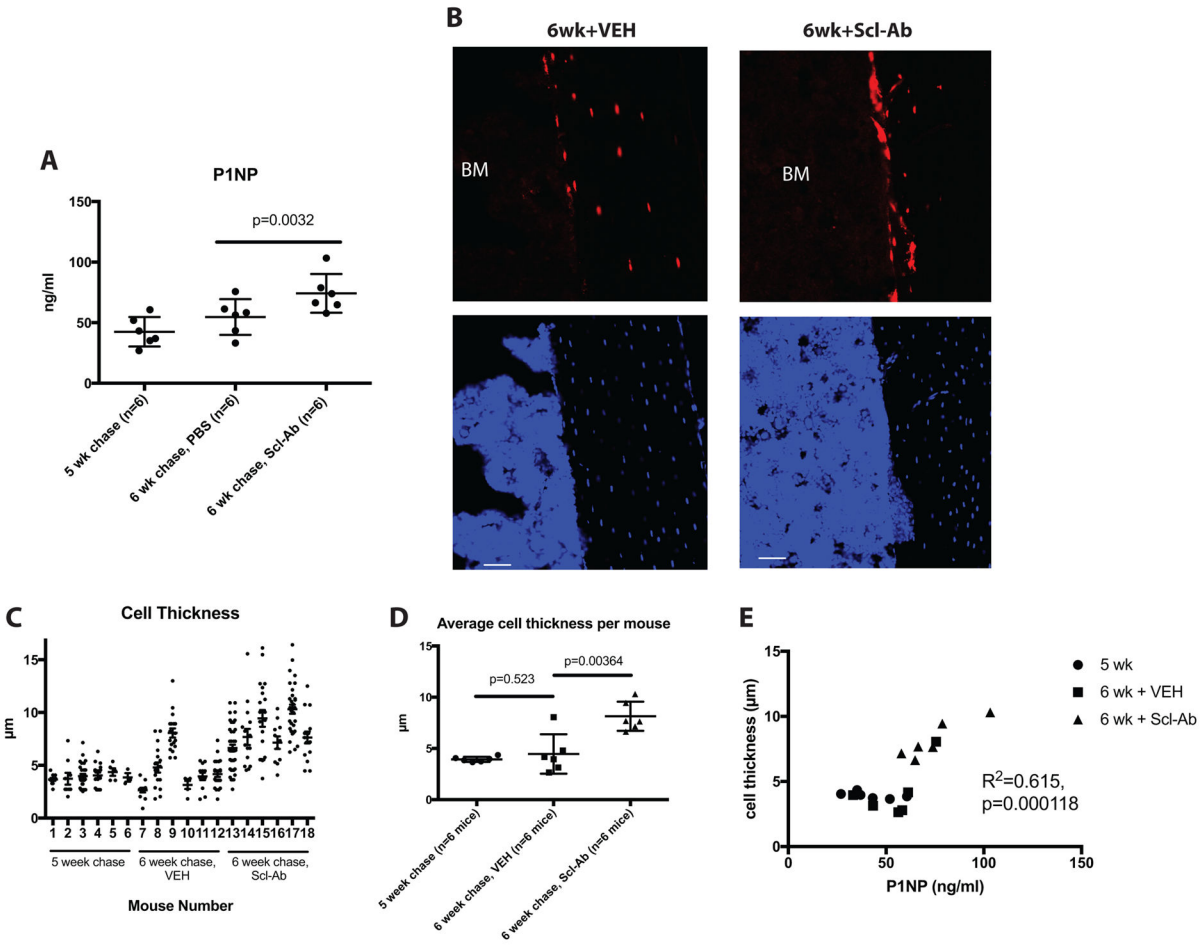

Figure 6. Scl-Ab treatment increases the thickness of tdTomato-positive endocortical cells

(A) Serum P1NP measurements from mice in the 3 indicated groups. Each data point represents an individual mouse, horizontal lines represent the mean, and error bars represent the standard deviation. **(B)** Representative 400x confocal images showing tdTomato signal in cells on endocortical surfaces of the tibia from the indicated experimental groups. Top images show red fluorescence from tdTomato, bottom images show DAPI stains. Scale bar=50 μm. **(C)** Cell thickness measurements of all endocortical tdTomato-positive cells observed on 2 sections per mouse. Each data point represents a different cell. **(D)** The mean cell thickness from each mouse is plotted amongst the 3 experimental groups, with p values comparing each group displayed on the graph. The relationship between serum P1NP and the average thickness of tdTomato-positive cells is shown. Circles represent mice from the 5 wk chase group, squares from the 6 wk + VEH cohort, and triangles from the 6 wk Scl-Ab-treated mice. R^2 and p values for linear regression analyses are shown on the graph.

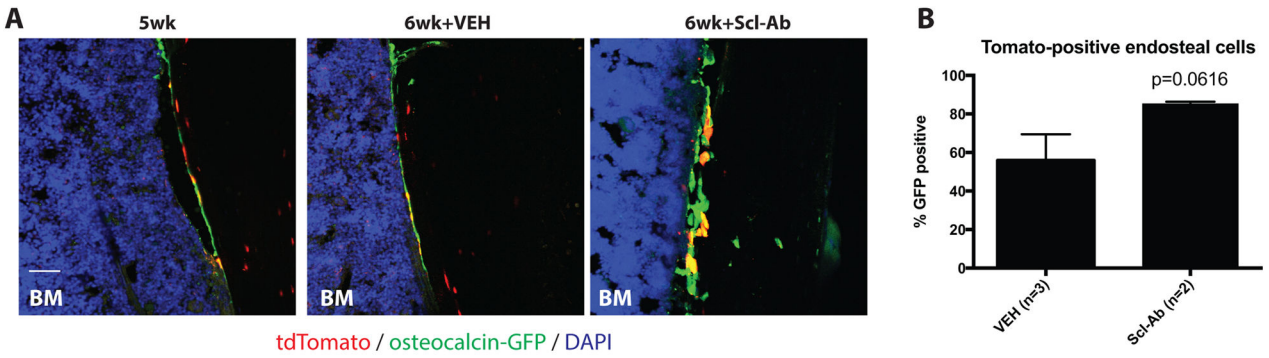

Figure 7. Scl-Ab increases osteocalcin expression in tdTomato-positive endocortical cells

(A) Confocal images from mice of the indicated treatment group showing osteocalcin and tdTomato expression in labeled cells on endocortical surfaces. In the 5wk and 6wk+VEH groups, many tdTomato-positive cells do not currently express osteocalcin. In contrast, in the 6wk+Scl-Ab group, more tdTomato-positive cells appear yellow due to concurrent osteocalcin-GFP expression. Scale bar=50 μm. **(B)** Quantification of GFP expression in tdTomato-positive endosteal cells.

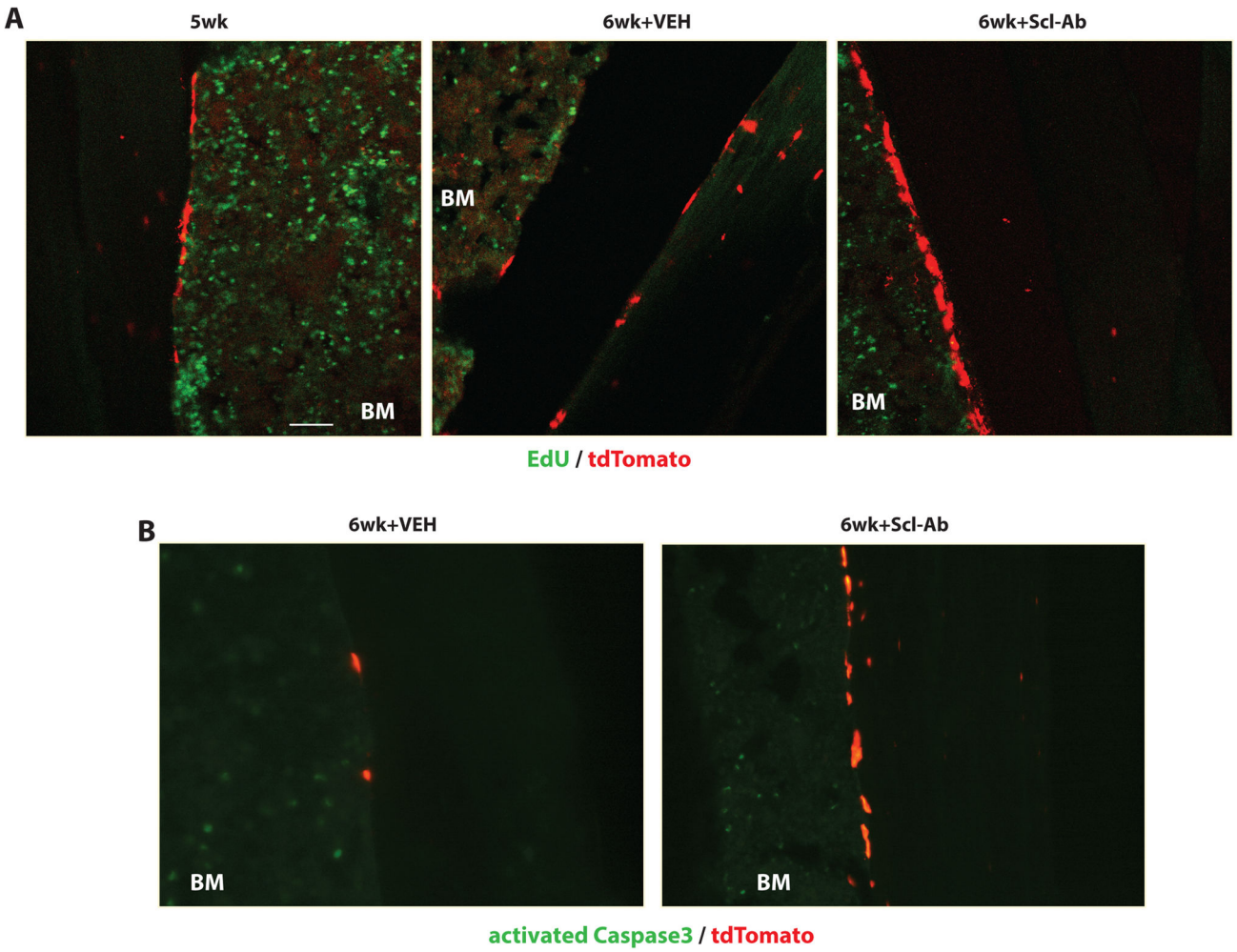

Figure 8. Scl-Ab treatment does not affect proliferation or apoptosis of endosteal lining cells

(A) 4 hours prior to sacrifice, mice were treated with EdU. Confocal images of sections for EdU and tdTomato. While many EdU-positive bone marrow cells were observed, no EdU-positive tdTomato-positive cells on bone surfaces were observed. Scale bar=50 μm. **(B)** Sections were stained with an antibody that recognizes activated caspase 3 (green). While many caspase-3-positive bone marrow cells were observed, no tdTomato-positive cells on bone surfaces stained positive for activated caspase 3 in any of the experimental groups.